Martian thermospheric warming associated with the Planet Encircling Dust Event of 2018

S. K. Jain[1], S. W. Bougher[2], J. Deighan[1], N. M. Schneider[1], F. González-Galindo[3], A. I. F. Stewart[1], R. Sharrar[2], D. Kass[4], J. Murphy[5], D. Pawlowski[6]

[1]Laboratory for Atmosphere and Space Physics, University of Colorado Boulder, Boulder, Colorado, USA
[2]Climate and Space Sciences and Engineering Department, University of Michigan, Ann Arbor, Michigan, USA.
[3]Instituto de AstrofÃnsica de Andalucía-CSIC, Granada, Spain
[4]Jet Propulsion Laboratory, California Institute of Technology, Pasadena, CA, USA
[5]Department of Astronomy, NMSU, Las Cruces, New Mexico, USA
[6]Department of Physics, Eastern Michigan University, Ypsilanti, Michigan, USA

Key Points:

- First observations of potential warming associated with a global dust storm
- Observations of meridional circulation in the thermosphere
- Temperature observations show breakdown of nominal circulation during the dust storm

Corresponding author: S. K. Jain, Sonal.Jain@lasp.colorado.edu

Abstract

We report the first observations of Martian thermospheric warming associated with the Planet Encircling Dust Event (PEDE) of 2018. We used dayglow observations made by the Imaging Ultraviolet Spectrograph instrument aboard the MAVEN spacecraft to retrieve the upper atmosphere temperature structures. Our analysis shows that the two-cell meridional circulation pattern may be operating before the PEDE-2018, which resulted in the cooling of lower/middle latitudes and warming at higher latitudes. However, after the onset the existing circulation pattern gets dampened, resulted in a weaker latitudinal temperature structure. We saw that mean temperatures rose by about 20 K for the same local time after the onset of the dust storm. Our 3D M-GITM (Mars General Ionosphere Thermosphere Model) calculations were able to reproduce the temperatures during the pre and early dust storm, but failed to fully capture the temperature trend during the growth phase of the PEDE of 2018.

1 Introduction

The coupled nature of Mars' lower and upper atmosphere requires crucial understanding of how a phenomenon such as regional and global dust storms affect thermospheric structure and dynamics. The effect of dust storms on the lower atmosphere has been studied in detail [*Smith et al.*, 2002; *Gurwell et al.*, 2005; *Cantor*, 2007; *Elteto and Toon*, 2010; *Heavens et al.*, 2011; *Kass et al.*, 2019]. However, dust storm effects on the dynamics, energetics, and circulation in the Martian thermosphere are not well understood due to insufficient observations of thermospheric temperatures during dust storm events. The measurements by Mariner 9, Mars Global Surveyor, and SPICAM have shown the responses due to dust storms by the thermospheric structure, especially the neutral and ionospheric densities [*Stewart and Hanson*, 1978; *Keating et al.*, 1998; *Bougher et al.*, 1999; *Forget et al.*, 2009; *Cox et al.*, 2010; *Withers and Pratt*, 2013]. The upper atmospheric expansion due to the dust storm was also observed in elevated airglow peak heights measured by the MAVEN Imaging Ultraviolet Spectrograph (IUVS) [*Gérard et al.*, 2019] and increased in neutral densities measured by the MAVEN Neutral Gas and Ion Mass Spectrometer (NGIMS) [*Liu et al.*, 2018; *Elrod et al.*, 2019]. *Forget et al.* [2009] reported temperatures from altitudes around 130 km using the SPICAM stellar occultation data, but did not report any significant effect of dust storms on the temperatures with exception of a few observations. However, the majority of their temperatures measurements were from the nightside.

The model simulations using three dimensional general circulation models (GCMs) have shown that significant dust loading in the lower atmosphere affects the circulation patterns in the upper atmosphere [e.g., *Bougher et al.*, 1999; *Bell et al.*, 2007; *Medvedev et al.*, 2013; *González-Galindo et al.*, 2015]. These model studies reported modification of the wind patterns in the thermosphere due to the dust loading, which in turn affects the interhemispheric Hadley circulation. The concomitant adiabatic heating gets modified by the radiative effects of vertical dust mixing ratio, and this effect is most prominent in the high latitudes [*Bougher et al.*, 1999; *Bell et al.*, 2007; *Medvedev et al.*, 2013; *González-Galindo et al.*, 2015]. *Bell et al.* [2007] used the Mars Thermospheric General Circulation Model (M-TGCM) to calculate the importance of dust loading in affecting the winter polar warming, thus emphasizing the role of lower atmospheric dust in the circulation and wind patterns in the upper atmosphere. *González-Galindo et al.* [2015] and *Medvedev et al.* [2013] have used the Laboratoire de Météorologie Dynamique - MGCM (LMD-MGCM) and Max Planck Mars GCM, respectively, to simulate the global dust storm in Mars years (MY) 25 and 28. For MY 25, *Medvedev et al.* [2013] predicted a decrease in the temperatures in the lower thermosphere at all latitudes except at very high polar latitudes. *González-Galindo et al.* [2015] predicted a cooling in low latitudes-mid in the lower thermosphere, but a warming at exobase levels at latitudes below 60°. For MY 28,

both models predicted significant warming at all latitudes except at northern polar region. Overall, all these models have shown the effect of dust storms in modifying the circulation and wind patterns in the upper atmosphere.

In this analysis, we are seeking to understand the impacts of the Planet Encircling Dust Event (PEDE) of 2018 on the thermospheric temperatures and its latitudinal structure and the implications of the underlying circulation patterns affecting the Mars thermosphere. This is the first global dust storm event since MAVEN went into orbit and it provided a unique opportunity to study its effect on the Mars upper atmosphere. We use dayglow observations made by the IUVS instrument to retrieve the upper atmosphere temperatures during the 2018 PEDE event. To understand the underlying dynamics, which in turn controls the temperatures, we use the Mars-Global Ionosphere Thermosphere Model (M-GITM) with the measured dust opacity for the 2018 PEDE event. The results presented in this analysis will help us constrain the potential role of lower atmospheric dust in altering the upper atmospheric circulation, which in turn may affect the temperatures.

2 Observation and Methodology

The planet encircling dust event (PEDE-2018) started around 1 June 2018 (Ls = 185°), as viewed in context imaging from the MRO/MARCI instrument [e.g., *Kass et al.*, 2019]. Enhanced temperatures were first noted in the middle atmosphere on 2-4 June (Ls = 186-187°) along with corresponding enhanced densities in the upper atmosphere on 8 June (Ls = 189°. The growth of the dust storm over the next 4-5 weeks (up to around 7 July, near Ls = 207°, witnessed the horizontal redistribution of dust around the planet, lofting dust up to ∼60-70 km, resulting in substantial warming of middle atmosphere temperatures (e.g. 50 Pa or ∼25-30 km) as observed by the MRO/MCS instrument [*Kass et al.*, 2019]. The PEDE of 2018 decayed thereafter until approximately mid-late October 2018 (Ls = 270-280°). Figure 1 shows the integrated optical depth measured by MRO/MCS, displayed as a function of latitude for 9 intervals distributed throughout the growth and initial decay phases of the PEDE-2018. This figure illustrates the time evolution of the PEDE dust opacities, which will be important in section 2.2 for describing the empirical dust distributions used for incorporation into model simulations.

2.1 Observations

We use dayglow measurements made by the Imaging Ultraviolet Spectrograph (IUVS) onboard the MAVEN spacecraft. IUVS takes 12 limb scans at the periapse segment of the MAVEN's orbit. The details of limb observations are provided in our earlier studies and the references therein [*McClintock et al.*, 2015; *Stevens et al.*, 2015; *Schneider et al.*, 2015; *Jain et al.*, 2018]. For the analysis presented in this paper, we use the CO_2^+ Ultraviolet Doublet (UVD) dayglow emission at 289 nm, which is one of the brightest mid-ultraviolet emissions in the Martian dayglow [*Jain et al.*, 2015; *Leblanc et al.*, 2006]. This emission is mainly produced by photon and electron impact ionization of CO_2 [*Jain and Bhardwaj*, 2012; *Gronoff et al.*, 2012] , making it an ideal diagnostic tool for retrieving information about the background neutral atmosphere [*Jain et al.*, 2015, 2018]. To retrieve scale heights and infer temperatures (at ∼170 km), we use an empirical Chapman fit to the CO_2^+ UVD emission intensity profile [*Lo et al.*, 2015; *Bougher et al.*, 2017]. We only use profiles for which the solar zenith angle is below 85 degrees. Another correction to the retrieved temperatures has been made for the profiles that are observed when the MAVEN spacecraft altitude was below 200 km. When the spacecraft is within the emitting layer, allowance must be made for the photons emitted "behind", and not seen by, the instrument. We used a simple Chapman layer model to examine the ratio of the signal seen by the instrument to the signal that would be seen from infinity along the same line-of-sight, for a range of exospheric temperatures, spacecraft altitudes above the emission peak to correct the emission profiles when the spacecraft is within the emitting layer. The
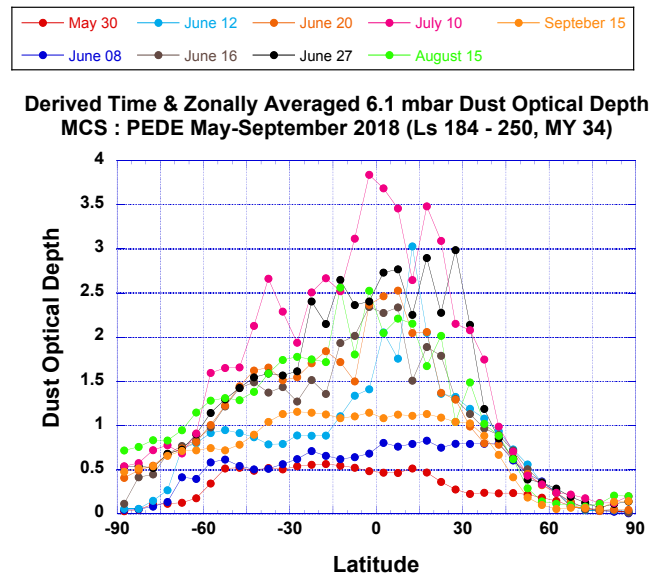
Figure 1. Integrated visible opacities from MCS are displayed as a function of latitude for 9 intervals distributed throughout the growth and initial decay phases of the PEDE-2018. These values are column integrated and are derived from the V5.2.7 MCS vertical dust distributions obtained during the PEDE-2018 period (e.g. Kass et al., 2019). Plotted values are time and zonally averaged (over all longitudes). These column integrated values are also fixed to a constant 6.1-mbar reference pressure surface. The dust opacity started slightly in the first week of June (coinciding with our storm onset data analysis of 25 May - 8 June), followed by a rapid growth phase in mid June (coinciding with second time period of 11-20 June considered in our study). The dust peaks around mid July (close to the third time period of 1-10 July considered in our analysis). The dust opacities followed a more gradual decline thereafter.

MAVEN orbit precesses with time to provide observations at different local time and latitudes. During the start of the PEDE-2018, the MAVEN periapsis was mostly sampling the southern hemisphere while it was approaching the dawn terminator from the morningside. The spacecraft was moving from low latitudes towards high S. hemisphere latitudes. Figure 2 shows the orbital evolution of the latitudes of all the profiles used in this analysis. The symbols are colored according to the local time of the observation.
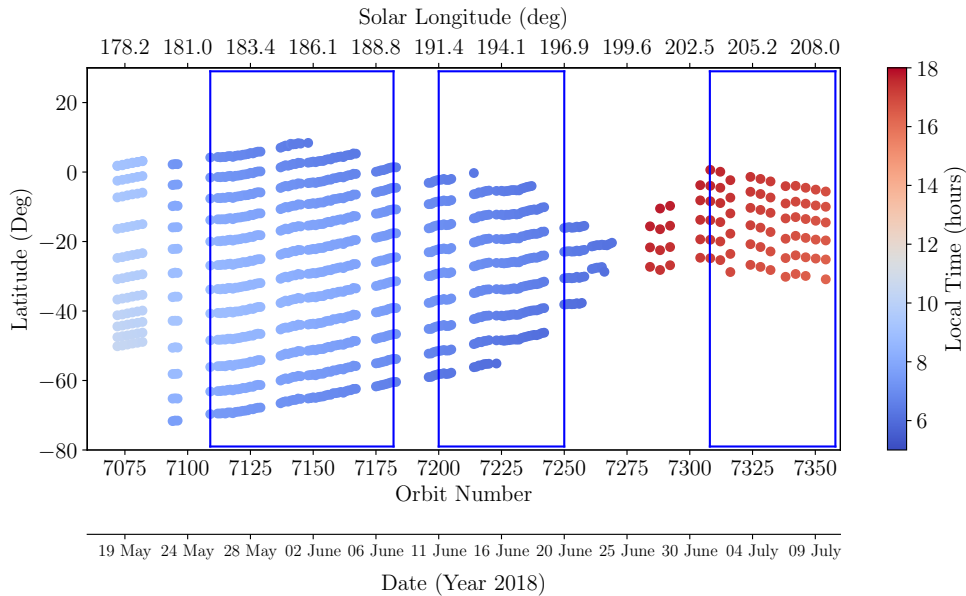
Figure 2. Evolution of latitudes at IUVS tangent points at the periapse with time (orbit numbers). The corresponding solar longitude and dates are shown in top and second bottom x-axis. The latitudes are colored according to the local time of the observations. The IUVS data is from May-July 2018. Three sampling intervals are illustrated for detailed data-model comparisons and subsequent analysis to be presented in sections 3 and 4.

Unfortunately, due to some observational limitations, the IUVS only took a few periapse observations before the start of the dust storm, with every even orbit between 7072 and 7082 (18-20 May 2018) and a few good orbits during 22-23 May 2018 (orbits 7094-7096). Starting from orbit 7109 (25 May 2018), the IUVS obtained good periapse observations with few gaps (due to a stellar occultation campaign and regular communication passes, and sharing time with other instruments onboard MAVEN), until the lighting conditions were not at all favorable (MAVEN periapsis had moved closer to the night side) to obtain the temperatures from the dayglow profiles.

As MAVEN periapsis was moving towards the dawn terminator, the side segment limb observations were moving towards lower solar zenith angle as shown in Figure 2. The inbound/outbound segment (side segment) of the MAVEN orbit is antipodal to the MAVEN periapse segment, which can provide dayside airglow measurements when MAVEN periapsis is on the nightside. The limb scans dusing the inbound/outbound segment are effectively similar to the periapse limb scans in terms of binning and have a similar data reduction process. The side segment limb observations, were taken around 17 hours Mars local time (compared to local time of 8 hours during the periapse limb observations). With both sets of limb scans, we could attempt to characterize the overall effects of the Martian PEDE-2018 storm on the upper atmosphere. The three sampling periods – PEDE-2018 onset (Ls = 181-189°), growth phase (Ls = 191-197 °), and the peak phase of PEDE-

2018 (Ls = 203-208 °) – are shown within the boxes and will be discussed in the following section to assess the impact of PEDE-2018 on Martian thermospheric temperatures.

2.2 MGITM model

The M-GITM code is a 3-D spherical model that was developed to address the physics of the entire Mars atmosphere system, capturing the basic observed features of the dynamical, thermal, and compositional structure of the atmosphere from ground to ~250 km [*Bougher et al.*, 2015]. The M-GITM framework was built from the terrestrial GITM framework [*Ridley et al.*, 2006], now utilizing Mars fundamental physical parameters, ion-neutral chemistry, and key radiative processes [*Bougher et al.*, 2015]. This ground to exosphere code is also constructed using existing physical formulations (e.g. CO_2 15-micron cooling, near IR heating, photochemistry) found in other modern Mars GCMs (see details in *Bougher et al.* [2015]). A fast and modern NLTE CO2 15-micron cooling scheme is now being used [e.g. Gonzalez-Galindo et al. 2013] to accurately compute CO2 cooling rates. Typically, M-GITM is setup to run with a $5° \times 5°$ latitude-longitude grid, using a 2.5 km vertical resolution.

Recent upgrades to the M-GITM code were tested and implemented to permit accurate solar irradiance and dust opacity inputs to be used for the PEDE-2018 simulations. First, the solar EUV-UV fluxes measured at Mars by the MAVEN Extreme Ultraviolet Monitor (EUVM) instrument have been used to generate daily averaged full solar spectra based upon the FISM-M (Flare Irradiance Spectral Model) empirical model [*Thiemann et al.*, 2017]. These daily averaged datasets provide solar EUV-UV fluxes to M-GITM corresponding to MAVEN measurements obtained during the PEDE-2018.

Second, model inputs are selected and utilized for time varying dust integrated optical depths and vertical dust distributions during the PEDE-2018. The latter are based upon available MRO/Mars Climate Sounder (MCS) dust opacity datasets (V5.2.7) [*Kleinböhl et al.*, 2009, 2011, 2017] as a function of MCS measured pressure intervals (up to 105) and zonally averaged latitude elements (36), thereby matching the M-GITM horizontal resolution. The resulting maps of vertical dust distribution are utilized to compute PEDE-2018 aerosol heating rates within the M-GITM code. These zonal averaged maps are derived from MCS opacity datasets for 9-reference time intervals chosen to correspond to milestones during the PEDE-2018 evolution (see Figure 1). Linear interpolation in time between these reference intervals is conducted, yielding vertical dust distributions that M-GITM uses throughout each simulated day. This time evolving dust scheme implemented within M-GITM, although based upon MCS measurements during the PEDE-2018, is a first order formulation and is subject to the availability of updated MCS products and how they are used. For instance, this initial dust formulation assumes dust is well mixed at low altitudes and can reasonably be zonally averaged.

Finally, temperatures corresponding to IUVS CO_2^+ UVD dayglow measurements are extracted from the M-GITM output datacubes throughout this PEDE-2018 period. An M-GITM flythrough routine is utilized for this extraction at each measurement location, yielding the corresponding M-GITM temperature at the same location.

3 Results

Figure 3 (a) shows the retrieved temperatures (at ~170 km) binned in latitude and solar longitude. As mentioned before, there was a limited amount of IUVS data just before the dust storm started, with slightly different local time. It is suggestive from the pre-dust storm data set that the latitudinal temperatures gradient was not large in magnitude. However, after Ls = 180° significant cooling at low latitudes resulted in a larger magnitude latitudinal temperature gradient through Ls = 190°, after which low latitude temperatures increased and the latitudinal gradient was reduced. As mentioned in Sec-
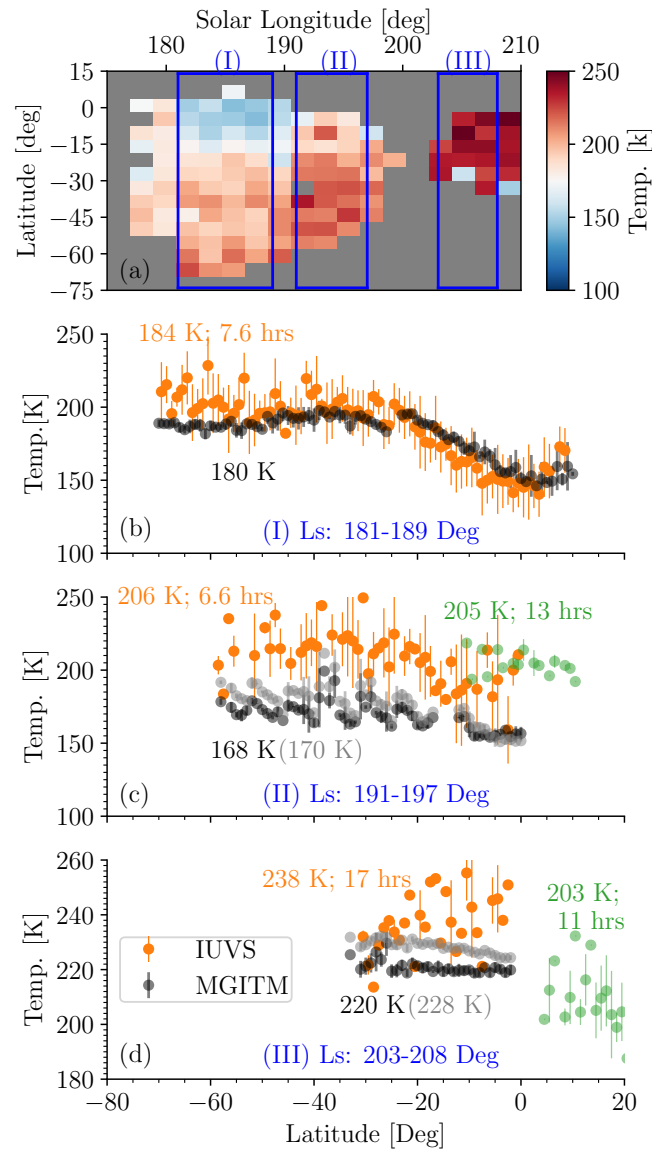
Figure 3. (a) The retrieved temperatures at ∼170 km from IUVS data in the time span shown in Figure 2. The temperatures are binned in solar longitude and geographic latitude grid. The three boxes (I, II, III) include the observational ranges where data-model comparison is performed and shown in subsequent panels as indicated by the corresponding roman numerals. (b) The longitudinally mean temperatures for Ls = 181–189° (orbit range: 7109-7182; date: 25 May - 8 June 2018 at the start of PEDE-2018 along with the 1-σ standard deviation. The orange symbols show the data from IUVS for the PEDE-2018. The black symbols are temperatures from M-GITM model (only for the PEDE-2018) extracted at similar local time, latitude, longitude and lighting conditions as described in Section 2.2 for the PEDE-2018 dust. The gray symbols are MGITM model runs for nominal dust optical depths (assuming no dust storm). The green symbol shows the observed temperatures from Martian year 33 for the same solar longitude range. (c) the longitudinally mean temperatures for Ls = 191-197°(orbit range: 7200-7250; date: 11 June - 20 June). (d) the longitudinally mean temperatures for Ls = 203-208° (orbit range: 7308-7358; date: 01 July - 10 July). The observed local time and the mean temperatures are shown in the panels for both IUVS and MGITM temperatures. The model values are only for MY34.

7

tion 2.1, the later orbits considered in this analysis were from early morning compared to those taken between Ls = 180 and 190°, however, the small difference in time might not able to explain this latitudinal behavior of thermospheric temperature. The temperatures retrieved from side segment limb scans around Ls = 205-208° show higher mean temperatures mostly because they are from afternoon hours, where Mars' thermospheric temperatures tend to be higher than the morning hours[*Stone et al.*, 2018]. These warmer afternoon temperatures are also simulated by the M-GITM model [*Bougher et al.*, 2015]. Unlike morning hours, the afternoon temperatures seem to be higher near the equator, with no significant latitudinal gradient.

Figure 3 (b) shows the longitudinally mean temperature after the onset/start of the dust storm. The figure contains data from IUVS observations made between 25 May - 8 June 2018 (Ls = 181–189°). The figure highlights the latitudinal gradient in the observed temperatures. Temperatures between -70° to -30° are 200-210 K, while at lower latitudes temperatures exhibit a substantial declining gradient to values of 145 K near the equator. The MGITM temperatures extracted for similar conditions as that of observations show that there is a very good agreement between the model and observed temperatures, and the model is able to reproduce the observed latitude gradient in the temperatures. This time period contains data at the very beginning of the dust storm as shown in Figure 1.

Figure 3 (c) shows the IUVS longitudinally mean temperatures from orbit 7200 to 7250 (Ls = 191–197°). By this time the dust storm has started to spread over the globe with significant increase in the dust optical depth(see Figure 1). Although, the mean local time during Ls = 191–197° was an hour earlier (6.6 hours) compared to the dust storm onset case (Ls = 181–189°), the mean observed temperature has increased by almost ~20 K. The temperatures also show large geophysical variability as shown by the error bars in the figure. The equatorial cooling has also diminished. The corresponding MGITM temperatures are shown in the same plot. Although, the latitudinal trend is roughly similar in both MGITM and IUVS temperatures, the model temperatures are underestimating the observations. The mean model temperatures are about ~35-40 K cooler (at high latitudes) than the mean IUVS temperatures, and ~12 K lower than for the pre-dust storm period. Near the equator, the model-IUVS temperatures are 20-30 K different.

The IUVS longitudinally mean temperatures for Ls = 203-208°(orbit: 7308-7358) are shown in Figure 3 (d). It is very difficult to infer a clear latitudinal trend in temperatures due to large variability observed in a given latitude bin, but the temperatures does indicate higher temperatures at equator region compared to those at 30-40° south. The average temperatures are about 238 K, larger than the previous two cases, but this could be due to the difference in the local time. During this time the dust optical depth was at its peak, which was included in this model run along with the solar forcing observed at Mars during this time. The overall M-GITM temperatures are ~50 K warmer than those for Ls = 191-197, in line with the difference between LT = 17 (evening terminator) and LT = 6.6 (morning terminator) sampling. This baseline difference in terminator temperatures (~40-50 K) is a non-dust storm feature of the observed and simulated atmosphere [e.g., *Bougher et al.*, 2015; *Stone et al.*, 2018]. Nevertheless, the dust-storm driven M-GITM temperatures (black dots) are underestimating the LT = 17 observations, with average temperatures are about 20 K cooler than the observations.

4 Discussion

Various numerical studies and recent observations have indicated that Mars atmosphere is an intimately coupled system, making it necessary to account for the lower atmosphere when modeling the structure and winds of the upper atmosphere [*Bell et al.*, 2007; *Lo et al.*, 2015; *Jain and Bhardwaj*, 2015]. In this regard, around the solstices, a single cell summer-to-winter inter-hemispheric mean Hadley circulation should exist, extending from the lower atmosphere to the thermosphere. For solstices, upwelling in the

summer hemisphere (leading to adiabatic cooling) and sinking (subsiding) in the winter hemisphere (yielding adiabatic warming) should occur. Alternatively, near the equinoxes, a double cell circulation pattern should exist, with rising motion (and adiabatic cooling) near the equator and subsiding motion (and adiabatic warming) at mid-to-high latitudes approaching both poles [*McCleese et al.*, 2010; *Bell et al.*, 2007]. Are these heating and cooling impacts observed in the changing longitudinally mean temperature versus latitude plots presented in Figure 3? If so, what do these impacts imply about the changing circulation patterns affecting the thermosphere, especially during the large events such as a global dust storm?

The thermospheric temperatures prior to Ls = 180° (see Figure 3 (a)) showed a weak solstitial meridional circulation (north to south). The temperatures started to decrease near the equator after Ls=180°. This suggests that a very different global circulation pattern is at work. A two-cell meridional circulation pattern may be operating, for which upwelling maximizes near the equator, thereby providing adiabatic cooling in this region. Conversely, the same meridional winds must sink (downwelling) at mid-to-high latitudes, providing adiabatic warming [*Bell et al.*, 2007; *González-Galindo et al.*, 2015]. The equatorial upwelling around Ls = 181-189 has a significant impact on the local temperatures (cooling effect) as shown in Figure 3 (b). Although, the dust opacities started to increase during this early PEDE-2018 period, (see Figure 1), they were relatively similar in magnitude to the climatological dust scenario at that time, and the model runs were also very similar.

Figure 3(c) shows an interesting case study during the growth phase of the PEDE-2018 (Ls = 191–197°). The observed temperatures are larger compared to pre-dust storm case, although they are measured one hour earlier in the morning. Also, the latitudinal temperature gradient is not as large in magnitude as it was during the PEDE-2018 onset case (Ls = 181–189°). Our model simulation using the M-GITM shows qualitative agreement with the observations in terms of the trend of the latitudinal distribution, but underestimated the measurements by an average of about 40 K. Moreover, M-GITM temperatures also failed to simulate the afternoon temperatures shown in Figure 3 (d), where the IUVS observed an average temperature of about 238 K compared to the simulated value of about 220 K. For this sampling period, M-GITM dust-driven upwelling winds increase in magnitude from the equator toward 30° south latitude, in accord with an enhanced meridional circulation (south to north) pattern owing to the dust storm. This yields relatively constant ~220 K temperatures from the equator to 30° (black dots).

The IUVS temperatures do show larger thermospheric temperatures during the global dust storm (Figure 3: panels (c), (d)) as predicted by earlier model calculations [*Medvedev et al.*, 2013; *González-Galindo et al.*, 2015]. To confirm whether this warming is associated with the dust storm, we have plotted thermospheric temperatures observed by IUVS during the nominal dust year of MY 33 (side segment data only; Date: 6 July 2016 - 21 Aug 2016; Orbit range: 3444-3694) in Figure 3 for the same solar longitudes as for the PEDE-2018. Although, local time and latitudinal coverage is not exactly similar during the two martian years, we could still try to understand the temperatures difference between the two years. During the growth phase (Ls=191-197°) of the PEDE-2018, the temperatures during the early dawn hours are similar in magnitude to that of afternoon temperature measured during the MY 33 (mean temperature is ~205). Given the diurnal cycle of thermospheric temperatures [*Stone et al.*, 2018], the apparent similar temperatures are actually indicating the possible thermospheric warming during the PEDE-2018. For the Ls = 208° (Figure 3 (d)), the PEDE-2018 temperatures are about 35K larger than that during the MY33. The local time difference (17 hrs for PEDE-2018 and 11 hrs for MY33) can not fully justify this difference because thermospheric temperature are supposed to be of the same magnitude during these times [*Stone et al.*, 2018]. The solar ionizing flux was about 15-20% larger during the MY 33, which should have resulted in higher thermospheric temperatures during the MY 33 not the opposite as we have seen in this analysis.

Although, comparative studies between MY 33 and MY34 would have been more helpful, if latitudinal and local time coverage had been similar, however, the available observations do suggest that the thermospheric warming may be associated with PEDE-2018.

González-Galindo et al. [2015] showed that the circulation gets damped at the thermopsheric altitudes by the development of the dust storm (which modifies the zonal and meridional winds at high altitudes), which in turn can modify the thermospheric temperatures. For simulations carried out for MY 25, which occured at similar solar longitude as the PEDE-2019, *González-Galindo et al.* [2015] reported a strong increase in the temperature at latitudes below 60 °, and decrease in temperature at polar latitudes during the peak of the storm. This scenario is similar to what IUVS observed during the peak of the PEDE-2019, where we observed higher temperatures near equator region. For MY28, *González-Galindo et al.* [2015] showed significant increase in exobase temperatures at all latitudes except at very high northern latitudes with the onset of dust storm. This increase in the exobase temperature in their simulation was not related to the solar forcing.

We also modeled the temperature using the climatological dust (outside any dust event) for both growth phase and peak of the PEDE-2018, which are shown in Figure 3 with gray symbols. The computed temperatures are up to ~10 K warmer for climatology dust, indicating that PEDE-2018 dust opacities are actually making the thermosphere colder in our M-GITM simulation. This is not in agreement with the earlier model calculations. The M-GITM model failed to capture the changing IUVS temperature versus latitude trends at 170 km during the PEDE-2018 event. This is most probably due to the lack of coupling between the lower and upper atmosphere via a gravity wave momentum and energy deposition mechanism that is presently not included in the MGITM simulations. This mechanism is likely responsible for modifying winds and temperature distributions in the Mars thermosphere, especially at mid-to-high latitudes [e.g., *Medvedev et al.*, 2013, 2015; *González-Galindo et al.*, 2015], thus affecting the MGITM model ability to accurately capture the dust storm thermospheric temperatures.

Withers and Pratt [2013] have studied the effect of dust storm on Mars' lower and upper atmosphere. Although, they didn't report any temperature observations, *Withers and Pratt* [2013] had inferred possible cooling in the upper atmosphere based on the apparent decrease in the density enhancement factor between 130 and 160 km using the MGS accelerometer data. A very recent study by *Liu et al.* [2018] has shown possible increase in thermospheric temperature related to local dust storms in MY 32 and MY 33. *Elrod et al.* [2019] have shown NGIMS densities and derived temperatures throughout the time evolution of the PEDE-2018 storm and reported slightly higher scale heights during the onset of the PEDE-2018, but no dayside temperatures were reported during the peak dust storm. This in-situ view is not easily compared to the remote IUVS temperatures described in this paper due to difference in the observing geometry. The latitude and altitudes in the NGIMS observations are coupled and can't be compared to latitudinal temperature distribution of IUVS. Due to the sparse and small number of Mars thermospheric observations during the global dust storm, we rely more on the GCMs to understand the thermospheric response to the PEDE. More observations of thermospheric temperatures in future would be really helpful in assessing the impact of the global dust storm from lower to upper atmosphere.

5 Summary and Conclusion

We present IUVS observations of thermospheric temperatures before and during the planet encircling dust event (PEDE-2018). Our analysis shows that the two-cell meridional circulation pattern may be operating before the PEDE-2018, which resulted in the cooling of lower/middle latitudes and warming at higher latitudes. The comparison between the observed temperatures during PEDE-2018 and MY 33 indicate that there is warming associated with the dust storm. The three dimensional general circulation model (M-GITM)

calculations were able to reproduce the temperatures during the dust storm onset, but failed to fully capture the temperature trend during the growth phase of the PEDE-2018. This could be due to the lack of any treatment of gravity waves in the MGITM. The extended spectral non-linear gravity wave parameterization of *Yiğit and Medvedev* [2009] and *Yiğit et al.* [2015] has recently been implemented within M-GITM and will be applied to updated PEDE-2018 simulations to carry this research forward. In addition, heat balance terms can be carefully examined for M-GITM simulations, yielding needed information about the role of the circulation in regulating the temperature structure. We also plan to perform detailed modeling by the LMD-GCM for the dust storm. The comparative study by two models may provide us better insight about the underlying circulation pattern in the upper atmosphere in the case of PEDE-2018 dust storm event.

References

Bell, J. M., S. W. Bougher, and J. R. Murphy (2007), Vertical dust mixing and the interannual variations in the Mars thermosphere, J. Geophys. Res., *112*(E12), E12002, doi: 10.1029/2006JE002856.

Bougher, S., G. Keating, R. Zurek, J. Murphy, R. Haberle, J. Hollingsworth, and R. T. Clancy (1999), Mars global surveyor aerobraking : atmospheric trends and model interpretation, *Advances in Space Research*, *23*(11), 1887–1897, doi:10.1016/S0273-1177(99)00272-0.

Bougher, S. W., D. Pawlowski, J. M. Bell, S. Nelli, T. McDunn, J. R. Murphy, M. Chizek, and A. Ridley (2015), Mars global ionosphere-thermosphere model: Solar cycle, seasonal, and diurnal variations of the mars upper atmosphere, *J. Geophys. Res.*, *120*(2), 311–342, doi:10.1002/2014JE004715, 2014JE004715.

Bougher, S. W., K. J. Roeten, K. Olsen, P. R. Mahaffy, M. Benna, M. Elrod, S. K. Jain, N. M. Schneider, J. Deighan, E. Thiemann, F. G. Eparvier, A. Stiepen, and B. M. Jakosky (2017), The structure and variability of mars dayside thermosphere from MAVEN NGIMS and IUVS measurements: Seasonal and solar activity trends in scale heights and temperatures, *J Geophys Res Space Phys*, *122*(1), 1296–1313, doi: 10.1002/2016ja023454.

Cantor, B. A. (2007), MOC observations of the 2001 Mars planet-encircling dust storm, Icarus, *186*(1), 60–96, doi:10.1016/j.icarus.2006.08.019.

Cox, C., J. C. Gérard, B. Hubert, J. L. Bertaux, and S. W. Bougher (2010), Mars ultraviolet dayglow variability: SPICAM observations and comparison with airglow model, *J. Geophys. Res.*, *115*, E04,010, doi:10.1029/2009JE003504.

Elrod, M., K. Roeten, S. W. Bougher, R. Sharrar, and J. Murphy (2019), Structural and compositional changes in the upper atmosphere related to the PEDE-2018
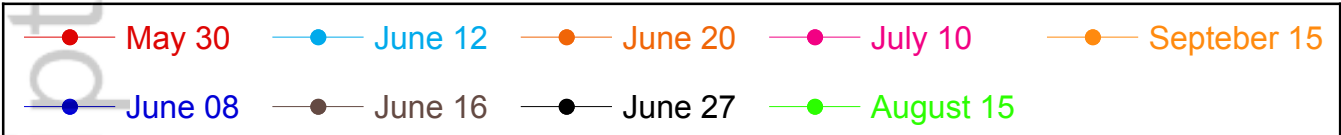
dust event on Mars as observed by MAVEN NGIMS, Geophys. Res. Lett., doi: 10.1029/2019GL084378.

Elteto, A., and O. B. Toon (2010), The effects and characteristics of atmospheric dust during martian global dust storm 2001A, Icarus, *210*(2), 589–611, doi: 10.1016/j.icarus.2010.07.011.

Forget, F., F. Montmessin, J. L. Bertaux, F. G. Galindo, S. Lebonnois, E. Quémerais, A. Reberac, E. Dimarellis, and M. A. L. Valverde (2009), Density and temperatures of the upper Martian atmosphere measured by stellar occultations with Mars Express SPICAM, *J. Geophys. Res.*, *114*, E01004, doi:10.1029/2008JE003086.

Gérard, J. C., L. Gkouvelis, B. Ritter, B. Hubert, S. K. Jain, and N. M. Schneider (2019), MAVEN-IUVS Observations of the CO_2^+ UV Doublet and CO Cameron Bands in the Martian Thermosphere: Aeronomy, Seasonal, and Latitudinal Distribution, J. Geophys. Res., doi:10.1029/2019JA026596.

González-Galindo, F., M. A. López-Valverde, F. Forget, M. García-Comas, E. Millour, and L. Montabone (2015), Variability of the Martian thermosphere during eight Martian years as simulated by a ground-to-exosphere global circulation model, J. Geophys. Res., *120*(11), 2020–2035, doi:10.1002/2015JE004925.

Gronoff, G., C. S. Wedlund, C. J. Mertens, M. Barthélemy, R. J. Lillis, and O. Witasse (2012), Computing uncertainties in ionosphere-airglow models. II - The Martian airglow, *J. Geophys. Res.*, *117*, A05309, doi:10.1029/2011JA017308.

Gurwell, M. A., E. A. Bergin, G. J. Melnick, and V. Tolls (2005), Mars surface and atmospheric temperature during the 2001 global dust storm, Icarus, *175*(1), 23–31, doi: 10.1016/j.icarus.2004.10.009.

Heavens, N. G., D. J. McCleese, M. I. Richardson, D. M. Kass, A. Kleinböhl, and J. T. Schofield (2011), Structure and dynamics of the Martian lower and middle atmosphere as observed by the Mars Climate Sounder: 2. Implications of the thermal structure and aerosol distributions for the mean meridional circulation, *Journal of Geophysical Research (Planets)*, *116*(E1), E01010, doi:10.1029/2010JE003713.

Jain, S. K., and A. Bhardwaj (2012), Impact of solar EUV flux on CO Cameron band and CO_2^+ UV doublet emissions in the dayglow of Mars, *Planet. Space Sci.*, *63-64*, 110 – 122, doi:10.1016/j.pss.2011.08.010.

Jain, S. K., and A. Bhardwaj (2015), Production of N_2 Vegard-Kaplan and Lyman-Birge-Hopfield emissions on Pluto, *Icarus*, *246*, 285–290, doi:10.1016/j.icarus.2014.08.032.

Jain, S. K., A. I. F. Stewart, N. M. Schneider, J. Deighan, A. Stiepen, J. S. Evans, M. H. Stevens, M. S. Chaffin, M. Crismani, W. E. McClintock, J. T. Clarke, G. M. Holsclaw, D. Y. Lo, F. Lefèvre, F. Montmessin, E. M. B. Thiemann, F. Eparvier, and B. M. Jakosky (2015), The structure and variability of Mars upper atmosphere as seen in MAVEN/IUVS dayglow observations, *Geophys. Res. Lett.*, *42*, 9023–9030, doi: 10.1002/2015GL065419.

Jain, S. K., J. Deighan, N. M. Schneider, A. I. F. Stewart, J. S. Evans, E. M. B. Thiemann, M. S. Chaffin, M. Crismani, M. H. Stevens, M. K. Elrod, A. Stiepen, W. E. McClintock, D. Y. Lo, J. T. Clarke, F. G. Eparvier, F. Lefévre, F. Montmessin, G. M. Holsclaw, P. C. Chamberlin, and B. M. Jakosky (2018), Martian Thermospheric Response to an X8.2 Solar Flare on 10 September 2017 as Seen by MAVEN/IUVS, *Geophys. Res. Lett.*, *45*, 7312–7319, doi:10.1029/2018GL077731.

Kass, D. M., J. T. Schofield, A. Kleinböhl, D. J. McCleese, N. G. Heavens, J. H. Shirley, and L. J. Steele (2019), Mars Climate Sounder observation of Mars' 2018 global dust event, Geophys. Res. Lett., doi:10.1029/2019GL083931.

Keating, G. M., S. W. Bougher, R. W. Zurek, R. H. Tolson, G. J. Cancro, S. N. Noll, J. S. Parker, T. J. Schellenberg, R. W. Shane, and B. L. Wilkerson (1998), The Structure of the Upper Atmosphere of Mars: In Situ Accelerometer Measurements from Mars Global Surveyor, *Science*, *279*, 1672, doi:10.1126/science.279.5357.1672.

Kleinböhl, A., J. T. Schofield, D. M. Kass, W. A. Abdou, C. R. Backus, B. Sen, J. H. Shirley, W. G. Lawson, M. I. Richardson, F. W. Taylor, N. A. Teanby, and D. J. Mc-

Cleese (2009), Mars Climate Sounder limb profile retrieval of atmospheric temperature, pressure, and dust and water ice opacity, J. Geophys. Res., *114*(E10), E10006, doi: 10.1029/2009JE003358.

Kleinböhl, A., J. T. Schofield, W. A. Abdou, P. G. J. Irwin, and R. J. de Kok (2011), A single-scattering approximation for infrared radiative transfer in limb geometry in the Martian atmosphere, J. Quant. Spec. Radiat. Transf., *112*, 1568–1580, doi: 10.1016/j.jqsrt.2011.03.006.

Kleinböhl, A., A. J. Friedson, and J. T. Schofield (2017), Two-dimensional radiative transfer for the retrieval of limb emission measurements in the martian atmosphere, J. Quant. Spec. Radiat. Transf., *187*, 511–522, doi:10.1016/j.jqsrt.2016.07.009.

Leblanc, F., J. Y. Chaufray, J. Lilensten, O. Witasse, and J.-L. Bertaux (2006), Martian dayglow as seen by the SPICAM UV spectrograph on Mars Express, *J. Geophys. Res.*, *111*, E09S11, doi:10.1029/2005JE002664.

Liu, G., S. L. England, R. J. Lillis, P. Withers, P. R. Mahaffy, D. E. Rowland, M. Elrod, M. Benna, D. M. Kass, D. Janches, and B. Jakosky (2018), Thermospheric Expansion Associated With Dust Increase in the Lower Atmosphere on Mars Observed by MAVEN/NGIMS, Geophys. Res. Lett., *45*(7), 2901–2910, doi:10.1002/2018GL077525.

Lo, D. Y., R. V. Yelle, N. M. Schneider, S. K. Jain, A. I. F. Stewart, S. England, J. Deighan, A. Stiepen, J. S. Evans, M. H. Stevens, M. S. Chaffin, M. Crismani, W. E. McClintock, J. T. Clarke, G. M. Holsclaw, and B. M. Jakosky (2015), Tides in the Martian Atmosphere as Observed by MAVEN IUVS, *Geophys. Res. Lett.*, *42*, 9057–9063, doi:10.1002/2015GL066268.

McCleese, D. J., N. G. Heavens, J. T. Schofield, W. A. Abdou, J. L. Bandfield, S. B. Calcutt, P. G. J. Irwin, D. M. Kass, A. Kleinböhl, and S. R. Lewis (2010), Structure and dynamics of the Martian lower and middle atmosphere as observed by the Mars Climate Sounder: Seasonal variations in zonal mean temperature, dust, and water ice aerosols, J. Geophys. Res., *115*(E12), E12016, doi:10.1029/2010JE003677.

McClintock, W. E., N. M. Schneider, G. M. Holsclaw, J. T. Clarke, A. C. Hoskins, I. Stewart, F. Montmessin, R. V. Yelle, and J. Deighan (2015), The Imaging Ultraviolet Spectrograph (IUVS) for the MAVEN Mission, *Space Sci. Rev.*, *195*, 75–124, doi: 10.1007/s11214-014-0098-7.

Medvedev, A. S., E. Yiğit, T. Kuroda, and P. Hartogh (2013), General circulation modeling of the Martian upper atmosphere during global dust storms, J. Geophys. Res., *118*(10), 2234–2246, doi:10.1002/2013JE004429.

Medvedev, A. S., F. González-Galindo, E. Yiğit, A. G. Feofilov, F. Forget, and P. Hartogh (2015), Cooling of the Martian thermosphere by CO_2 radiation and gravity waves: An intercomparison study with two general circulation models, J. Geophys. Res., *120*(5), 913–927, doi:10.1002/2015JE004802.

Ridley, A. J., Y. Deng, and G. Tóth (2006), The global ionosphere thermosphere model, *J. Atmos. Sol. Terr. Phys.*, *68*, 839–864, doi:10.1016/j.jastp.2006.01.008.

Schneider, N. M., J. Deighan, A. I. F. Stewart, W. E. McClintock, S. K. Jain, M. H. Chaffin, A. Stiepen, M. Crismani, J. Plane, J. D. C. Sanchez, J. S. Evans, M. H. Stevens, R. V. Yelle, J. T. Clarke, G. M. Holsclaw, F. Montmessin, and B. M. Jakosky (2015), MAVEN IUVS Observations of the Aftermath of Comet Siding Spring's Meteor Shower, *Geophys. Res. Lett.*, *42*, doi:10.1002/2015GL063863.

Smith, M. D., B. J. Conrath, J. C. Pearl, and P. R. Christensen (2002), NOTE: Thermal Emission Spectrometer Observations of Martian Planet-Encircling Dust Storm 2001A, Icarus, *157*(1), 259–263, doi:10.1006/icar.2001.6797.

Stevens, M. H., J. S. Evans, N. M. Schneider, A. I. F. Stewart, J. Deighan, S. K. Jain, M. Crismani, A. Stiepen, M. S. Chaffin, W. E. McClintock, G. M. Holsclaw, F. Lefèvre, D. Y. Lo, J. T. Clarke, F. Montmessin, and B. M. Jakosky (2015), N_2 in the upper atmosphere of Mars observed by IUVS on MAVEN, *Geophys. Res. Lett.*, *42*, 9050–9056, doi:10.1002/2015GL065319.

Stewart, A. I., and W. B. Hanson (1978), Mars upper atmosphere - Mean and variations, in *The Mars Reference Atmosphere*, edited by A. Kliore, pp. 113–132, doi:10.1016/0273-1177(82)90109-0.

Stone, S. W., R. V. Yelle, M. Benna, M. K. Elrod, and P. R. Mahaffy (2018), Thermal structure of the martian upper atmosphere from maven ngims, *J. Geophys. Res.*, doi: 10.1029/2018JE005559.

Thiemann, E. M. B., P. C. Chamberlin, F. G. Eparvier, B. Templeman, T. N. Woods, S. W. Bougher, and B. M. Jakosky (2017), The MAVEN EUVM model of solar spectral irradiance variability at Mars: Algorithms and results, J. Geophys. Res., *122*(3), 2748–2767, doi:10.1002/2016JA023512.

Withers, P., and R. Pratt (2013), An observational study of the response of the upper atmosphere of Mars to lower atmospheric dust storms, *Icarus*, *225*, 378–389, doi: 10.1016/j.icarus.2013.02.032.

Yiğit, E., and A. S. Medvedev (2009), Heating and cooling of the thermosphere by internal gravity waves, Geophys. Res. Lett., *36*(14), L14807, doi:10.1029/2009GL038507.

Yiğit, E., S. L. England, G. Liu, A. S. Medvedev, P. R. Mahaffy, T. Kuroda, and B. M. Jakosky (2015), High-altitude gravity waves in the Martian thermosphere observed by MAVEN/NGIMS and modeled by a gravity wave scheme, Geophys. Res. Lett., *42*(21), 8993–9000, doi:10.1002/2015GL065307.

Figure 1.

Derived Time & Zonally Averaged 6.1 mbar Dust Optical Depth
MCS : PEDE May-September 2018 (Ls 184 - 250, MY 34)

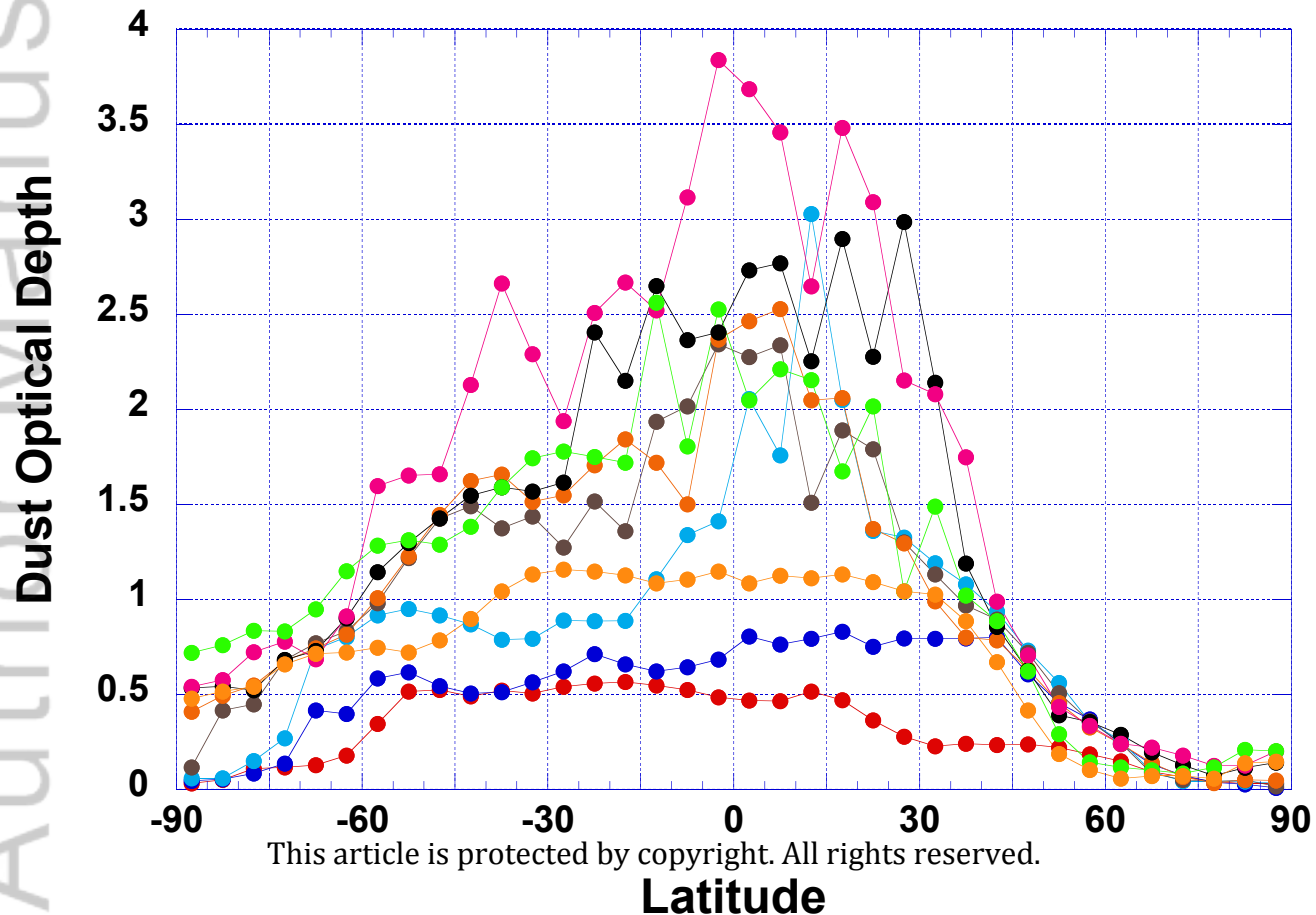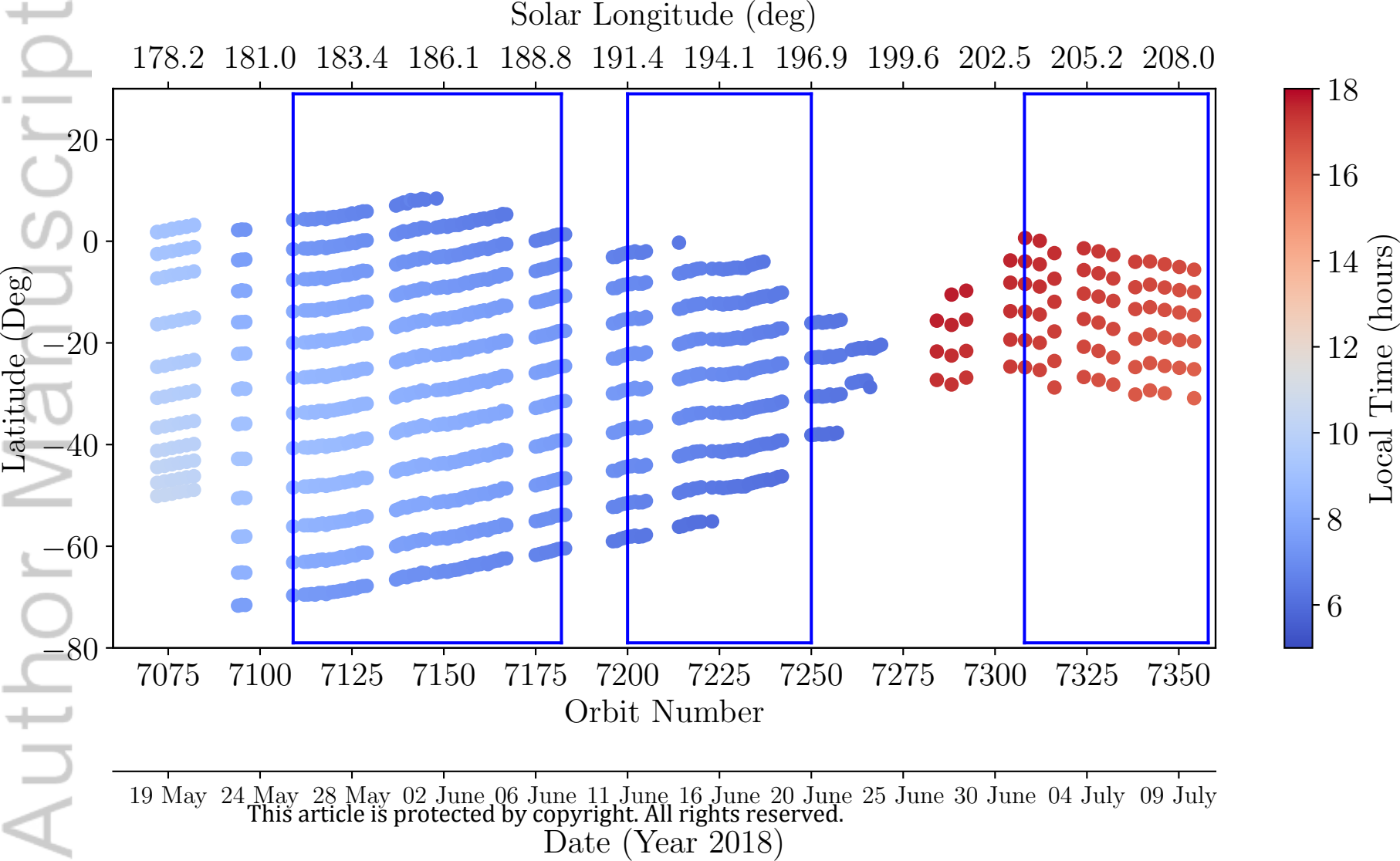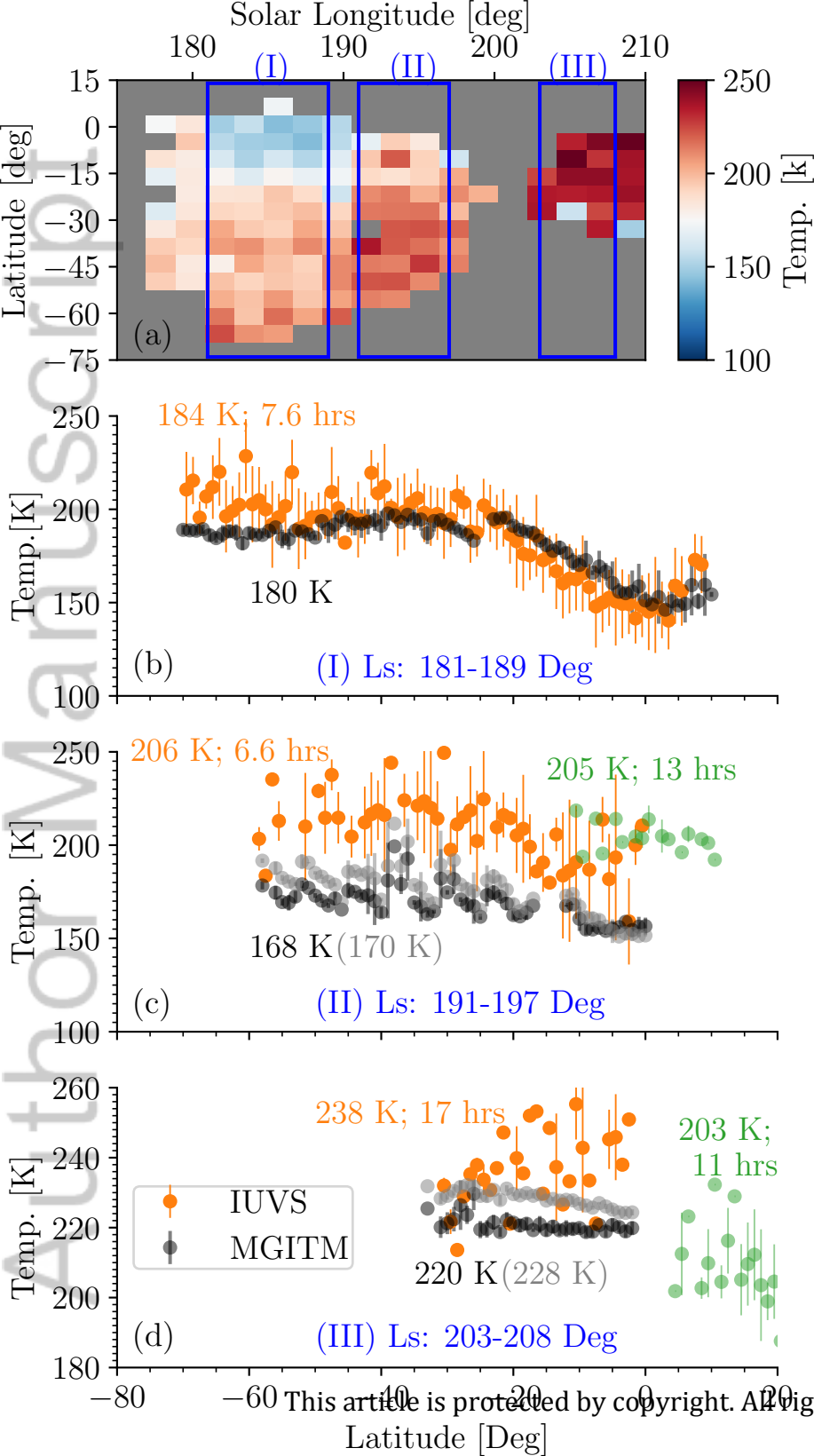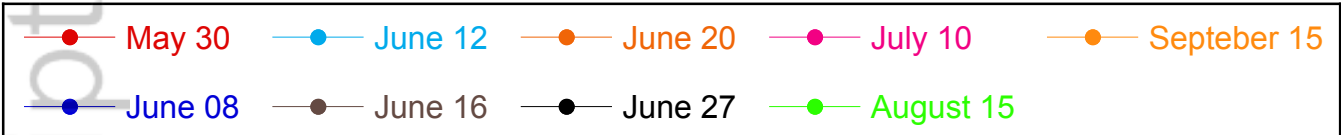Legend: May 30, June 12, June 20, July 10, Septeber 15, June 08, June 16, June 27, August 15

Figure 2.

Figure 3.

Derived Time & Zonally Averaged 6.1 mbar Dust Optical Depth
MCS : PEDE May-September 2018 (Ls 184 - 250, MY 34)

Legend:
- May 30
- June 12
- June 20
- July 10
- Septeber 15
- June 08
- June 16
- June 27
- August 15

Y-axis: Dust Optical Depth
X-axis: Latitude